Optimal control of the generalized Kuramoto-Sivashinsky equation with energy- and entropy-based objectives

Hiroya Mamori *
Department of Mechanical and Intelligent Systems Engineering, The University of Electro-Communications, Tokyo, Japan

Yusuke Nabae
Department of Mechanical Systems Engineering, Tokyo Metropolitan University and Department of Mechanical Engineering, Tokyo University of Science, Tokyo, Japan

Hiroshi Gotoda
Department of Mechanical Engineering, Tokyo University of Science, Tokyo, Japan

(Received 25 March 2026; accepted 13 August 2026; published 4 September 2026)

We conduct numerical simulations of a noisy generalized Kuramoto-Sivashinsky system under optimal control. The cost functions are kinetic energy and permutation entropy, which are designed to reduce the kinetic energy and the permutation entropy, respectively. The results demonstrate that kinetic-energy-based control strongly suppresses the structures and drives the system into a trivial state. In contrast, the permutation-entropy-based control preserves nontrivial structures, although the reduction in kinetic energy is smaller and requires only slight actuation energy. These findings provide insight into designing control strategies for complex systems where both efficiency and functional richness are desired.

DOI: 10.1103/b2h7-b2qs

I. INTRODUCTION

Many physical and engineering systems, e.g., turbulent flows, combustion, and chemical reaction-diffusion systems, exhibit complex spatiotemporal dynamics driven by the interplay between nonlinear interactions, dissipation, and external forcing. These systems are often modeled by active-dissipative partial differential equations that can display chaotic behavior, especially in the presence of noise.

The Kuramoto-Sivashinsky (KS) equation is one of the well-recognized prototypical models describing complex spatiotemporal dynamics. The KS equation was derived by Kuramoto and Tsuzuki [1] and Sivashinsky [2] in the context of the phase turbulence in reaction-diffusion systems and wrinkled flame front propagation, respectively. It includes nonlinear advection, second- and fourth-order derivative terms, and is known to produce high-dimensional chaotic states or low-dimensional coherent structures depending on the relative strength of its parameters. The KS equation can be also derived as a weakly nonlinear approximation of one-dimensional flow dynamics for falling-film flows. The generalized Kuramoto-Sivashinsky (gKS) equation, i.e., the KS equation with a dispersion term, has been used to analyze wave evolution in thin films. Gotoda *et al.* [3,4] investigated the temporal chaotic behavior generated by one-dimensional KS and gKS equations. Furthermore, they assessed the prediction performance of the nonlinear forecasting for these equations.

The gKS equation is suitable for analyzing the complex spatiotemporal dynamics. Likewise, the control of the dynamics is a challenging issue and an optimal control theory has provided promising tools for systematically designing control inputs for complex spatiotemporal dynamics. Although the turbulent flow shows strong nonlinearity, Bewley *et al.* [5] successfully demonstrated that optimal wall-normal blowing and suction can lead to relaminarization of turbulent channel flow. The control input based on optimal control theory is designed to minimize a prescribed cost functional. This approach effectively suppresses the fluctuations by minimizing the total kinetic energy in the flow. In accordance, Yamamoto *et al.* [6] have shown the dissimilar control effect for momentum and heat transfer in the turbulent flow through the optimal control theory. The resultant control input is similar to the traveling wave propagating in the streamwise direction.

Despite their effectiveness in suppressing turbulence, these control strategies can also eliminate beneficial aspects of turbulence, such as enhanced mixing. In other words, while minimizing kinetic energy may reduce drag or energy dissipation, it may also lead to an undesired degradation of system functionality. For example, Bewley's control [5] significantly modulates the flow structure; namely, relaminarization is one example of a trivial state in which the turbulence is perfectly absent; in the traveling-wave controlled flow by Yamamoto *et al.* [6], the turbulence remains while the spanwise rollerlike rotation dominates the flow. Therefore, an important question arises: can we design control strategies that preserve the

*Contact author: mamori@uec.ac.jp; http://www.mamorilab.mi.uec.ac.jp

richness of the system dynamics while still reducing energy consumption?

In this study, we address this question using the gKS equation as a model of an active-dissipative system under the influence of external noise. Two types of optimal control strategies are formulated based on adjoint methods: one that minimizes the total kinetic energy of the system, and another that minimizes the information entropy of the system as measured by the permutation patterns [7,8]. The kinetic energy-based control is quadratic and yields an analytical expression for the optimal forcing, whereas the entropy-based-control is nonquadratic and requires a steepest-descent iteration. By comparing these two control strategies, we aim to reveal the trade-off between energy suppression and preservation of dynamical structure.

We employ the gKS equation as a model of a nonlinear active-dissipative system to develop an entropy-based optimal control strategy. The gKS equation was originally derived under a long-wave approximation to describe pattern formation in thin-film flows and its applicability is physically limited to slow viscous flows and interfacial dynamics. Here, we treat the gKS equation not as a physically faithful representation of wall turbulence, but rather as a canonical system that exhibits essential dynamical features. It should be emphasized that our intention is not to apply the proposed control framework directly to turbulent channel flows in its current form. Instead, the gKS equation provides a mathematically tractable platform for exploring the underlying principles of spatiotemporal control in nonlinear systems, which may eventually inform more physically realistic turbulence control strategies.

The rest of this paper is organized as follows. In Sec. II, we introduce the governing equation, cost functionals, and numerical implementation of the optimal control strategies. Section III presents the simulation results and comparative analysis. Finally, Sec. IV summarizes the key findings and discusses implications for broader applications.

II. NUMERICAL SIMULATION AND CONTROL INPUT

The governing equation is the generalized Kuramoto-Sivashinsky (gKS) equation with noise and the control, which reads

$$\frac{\partial u}{\partial t} + u\frac{\partial u}{\partial x} + \frac{\partial^2 u}{\partial x^2} + \delta\frac{\partial^3 u}{\partial x^3} + \nu\frac{\partial^4 u}{\partial x^4} + \sigma\zeta = f. \tag{1}$$

Here, $u = u(x,t)$ denotes the state variable dependent on spatial coordinate x and time t. The nonlinear convective term captures the self-interaction of the state variable, while the third and fourth derivative terms account for the dispersion and damping, which affect the stability and evolution of the system. The parameters δ and ν are associated with dispersion and damping effects, respectively. The term $\zeta = \zeta(x,t)$ represents a stochastic or random function defined from 0 to 1, introducing noise into the system. Its amplitude is controlled by the parameter σ, which quantifies the intensity of the stochastic perturbations. The function $f = f(x,t)$ serves as the control input, enabling manipulation of the dynamics in the system to achieve desired states or behaviors. The periodic boundary condition is imposed in the x direction.

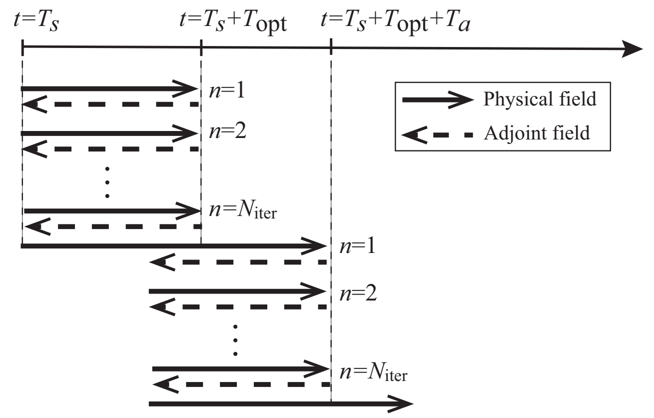

FIG. 1. Schematic of optimizing the control input in the case of J_K and J_{h_p}.

We compute the control input f based on the optimal control theory. The Lagrangian $\mathcal{L}$ is defined as

$$\mathcal{L} = J + \int_{T_s}^{T_s+T_{\rm opt}} \int_0^{L_x} \lambda(x,t) \left(\frac{\partial u}{\partial t} + u\frac{\partial u}{\partial x} + \frac{\partial^2 u}{\partial x^2} + \delta\frac{\partial^3 u}{\partial x^3} + \nu\frac{\partial^4 u}{\partial x^4} + \sigma\zeta - f\right) dx\, dt \tag{2}$$

Here, J is the cost function and $\lambda(x,t)$ is the adjoint variable. In this study, we investigate two different objective functions, i.e., J_K and J_{h_p}. The first one includes the kinetic energy u^2 as

$$J_K = \frac{1}{2}\int_{T_s}^{T_s+T_{\rm opt}} \int_0^{L_x} u^2\, dx\, dt + \frac{\alpha}{2}\int_{T_s}^{T_s+T_{\rm opt}} \int_0^{L_x} f^2\, dx\, dt. \tag{3}$$

Here, α is the weight for the control cost, which is set to be $\alpha = 1$. The cost function aims to decrease the kinetic energy and the control cost from $t = T_s$ to $t = T_s + T_{\rm opt}$ as shown in Fig. 1. The adjoint equation is obtained from the condition of $\delta\mathcal{L}/\delta u = 0$, i.e.,

$$\frac{\partial \lambda}{\partial t} + u\frac{\partial \lambda}{\partial x} - \frac{\partial^2 \lambda}{\partial x^2} + \delta\frac{\partial^3 \lambda}{\partial x^3} - \nu\frac{\partial^4 \lambda}{\partial x^4} + \lambda\frac{\partial u}{\partial x} = u. \tag{4}$$

The adjoint equation is solved in backward time with the termination condition, e.g., from $t = T_s + T_{\rm opt}$ to $t = T_s$ with $\lambda(x, T_s + T_{\rm opt}) = 0$. The periodic boundary condition is also imposed for λ. Owing to a quadratic function of J_K, the optimal control input can be theoretically derived from $\partial\mathcal{L}/\partial f = 0$, as

$$f = \frac{1}{\alpha}\lambda. \tag{5}$$

Therefore, we can compute the control input from the adjoint variable straightforwardly.

Another objective function aims to decrease the permutation entropy, which reads

$$J_{h_p} = \int_{T_s}^{T_s+T_{\rm opt}} h_p dt + \frac{\alpha}{2}\int_{T_s}^{T_s+T_{\rm opt}} \int_0^{L_x} f^2\, dx\, dt. \tag{6}$$

The permutation entropy [8] of u is defined as

$$h_p = -\sum_{\pi_i} p_e(\pi_i) \ln p_e(\pi_i) / \ln D_e!,$$

where p_e is the probability of a permutation pattern $\pi_i (i = 1, 2, \ldots, D_e!)$ and D_e is the embedding dimension. In this study, the permutation patterns are investigated for spatial distribution of u, and therefore h_p is a function of time t. Decreasing D_e tends to make the reconstructed attractor more sensitive to noise, potentially approaching the characteristics of stochastic signals such as noise. The sampling interval is the grid spacing, i.e., $\Delta x = L_x/N_x$. In the reference cases, the length of the computational domain is $0 \leqslant x \leqslant L_x$ with $L_x = 1000$, and the corresponding number of grid points is $N_x = 2048$.

The adjoint equation is obtained as

$$\frac{\partial \lambda}{\partial t} + u\frac{\partial \lambda}{\partial x} - \frac{\partial^2 \lambda}{\partial x^2} + \delta\frac{\partial^3 \lambda}{\partial x^3} - \nu\frac{\partial^4 \lambda}{\partial x^4} + \lambda\frac{\partial u}{\partial x} = \frac{\partial h_p}{\partial u}, \quad (7)$$

with the termination condition $\lambda(x, T_s + T_{\mathrm{opt}}) = 0$. From the condition of $\partial\mathcal{L}/\partial f = 0$, the cost function gradient reads

$$\frac{\partial J_{h_p}}{\partial f} = \alpha f - \lambda. \quad (8)$$

Here, $\partial h_p/\partial u$ is numerically evaluated by finite perturbation of the state variable as

$$\frac{\partial h_p}{\partial u} = \frac{h_p(u+\varepsilon) - h_p(u)}{\varepsilon}, \quad (9)$$

where ε is the perturbation amplitude. A steepest descent method is used to update the control input as

$$f^{n+1} = f^n - \eta(\alpha f^n - \lambda), \quad (10)$$

where η is the step size in the steepest descent update, set to $\eta = 1$. The superscript n means the nth substep in N_{iter} as shown in Fig. 1.

We employed an in-house code based on Fukagata *et al.* [9] to solve the gKS equation. For spatial discretization of the governing equation, an energy conservative second-order accurate central difference method [10,11] was employed. For temporal integration of the gKS equation, a low-storage third-order accurate Runge-Kutta scheme was used. The simulation starts from noisy fields in the uncontrolled case and fully developed fields in the controlled case. The control starts at $t = 0$.

The control effect is evaluated by time-averaged kinetic energy and permutation entropy, as

$$\overline{K} = \frac{1}{L_x(\mathcal{T}_2 - \mathcal{T}_1)}\int_{\mathcal{T}_1}^{\mathcal{T}_2}\int_o^{L_x}\frac{u'u'}{2}dx\,dt, \quad (11)$$

$$\overline{h_p} = \frac{1}{\mathcal{T}_2 - \mathcal{T}_1}\int_{\mathcal{T}_1}^{\mathcal{T}_2} h_p(t)dt, \quad (12)$$

respectively. The prime indicates the fluctuation from the spatial averaging,

$$u'(x,t) = u(x,t) - \frac{1}{L_x}\int_0^{L_x} u(x,t)\,dx. \quad (13)$$

The averaging time is from $\mathcal{T}_1$ to $\mathcal{T}_2$ at a fully developed state.

Figure 2 shows the spatiotemporal patterns of $u(x,t)$ for different δ at fixed σ without any control. For $\delta = 0$, we observe a disorderedlike pattern exhibiting high-dimensional chaotic dynamics. The noise disappears with the increasing δ, leading to the emergence of coherent patterns, which gives low-dimensional chaos. Since the spatiotemporal patterns are in reasonable agreement with Gotoda *et al.* [4], the present simulation can reproduce the spatiotemporal patterns in the noisy gKS equation.

TABLE I. Verification of simulation at $\delta = 0.2$, $\sigma = 1.0$, and $\nu = 1$. Values in parentheses indicate cases in which the sampling interval differs from that in the reference and large-domain cases.

Objective function	L_x	N_x	D_e	N_{iter}	T_{opt}	T_a	$\overline{K}$	$\overline{h_p}$
	1000	2048	4				1.09	0.502
	2000	4096	4				1.06	0.499
	1000	4096	4				0.973	(0.378)
J_K	1000	2048	4	3	0.4	0.2	0.175	0.454
J_K	2000	4096	4	3	0.4	0.2	0.168	0.453
J_K	1000	4096	4	3	0.4	0.2	0.154	(0.350)

Verification of the simulation is summarized in Table I. Three computational conditions are considered: the reference domain ($L_x = 1000$, $N_x = 2048$), a large domain ($L_x = 2000$, $N_x = 4096$, with the same spatial resolution as the reference case), and a high-resolution domain ($L_x = 1000$, $N_x = 4096$). In the uncontrolled cases, the differences in $\overline{K}$ and $\overline{h_p}$ between the reference and large-domain cases are small. We note that, in the high-resolution case, $\overline{h_p}$ differs because the sampling interval (i.e., the grid spacing) is half that of the reference and large-domain cases. Since h_p depends on the sampling interval used in the ordinal-pattern analysis, these values are not directly comparable and are therefore shown in parentheses. In the controlled cases with the objective function J_K, the differences in $\overline{K}$ are also small, while the parenthesized $\overline{h_p}$ value should again be interpreted with care for the same reason. Therefore, the effects of the domain size and spatial resolution are small in the present simulations. In the following, we employ the reference domain with $L_x = 1000$ and $N_x = 2048$.

Figure 3 shows the impulse-response test for the case of J_{h_p} at $D_e = 4$, $N_{\mathrm{iter}} = 4$, $T_{\mathrm{opt}} = 0.4$, and $T_a = 0.2$ computed in the reference domain. Over the tested range of perturbation amplitude ε, both $\overline{K}$ and $\overline{h_p}$ exhibit little significant variation. This indicates that the numerical evaluation of $\partial h_p/\partial u$ is largely insensitive to the choice of perturbation amplitude in the present setting. Therefore, we chose the impulse response of $\varepsilon = 1.0$ in the following.

III. RESULTS AND DISCUSSION

We investigate the effect of the optimization parameters on $\overline{K}$ and $\overline{h_p}$. The three uncontrolled cases and the eight different control cases are chosen as summarized in Table II. In the uncontrolled cases, as D_e increases, $\overline{h_p}$ decreases. In the controlled cases, the flow parameters are the same at $\delta = 0.2$, $\sigma = 1.0$, and $\nu = 1$. In Cases A–E, the objective function is J_K. As compared with Case B, N_{iter} is different in Cases A and C; T_{opt} and T_a are different in Cases D and E, respectively. $\overline{K}$ and $\overline{h_p}$ in Cases A–C are in good agreement with each other. The number of iteration N_{iter} and the time advance T_a hardly affects $\overline{K}$ and $\overline{h_p}$. In Case D where T_{opt} and T_a are doubled, $\overline{K}$ is significantly smaller and $\overline{h_p}$ is larger than other cases.

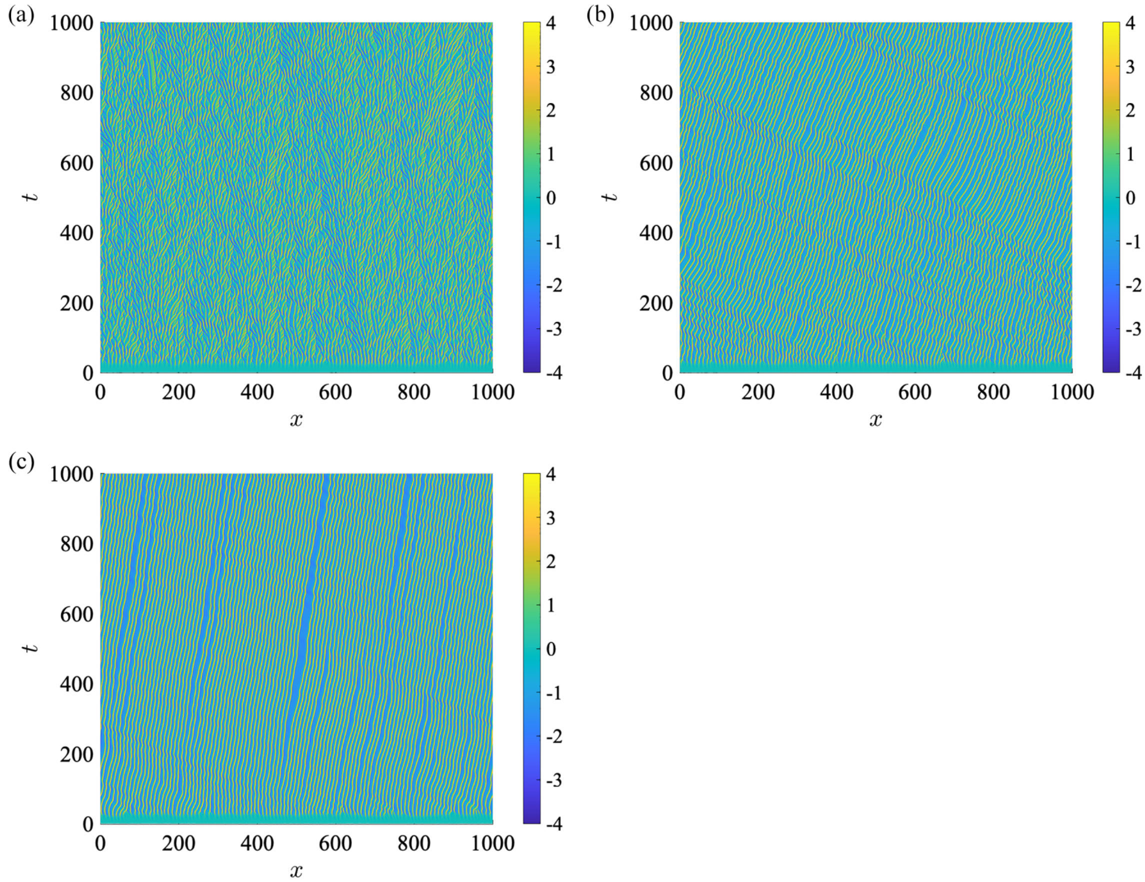

FIG. 2. Spatiotemporal patterns of $u(x,t)$ in the noisy gKS solution for different δ without control at $\sigma = 0.06$ and $\nu = 1$: (a) $\delta = 0$, (b) $\delta = 0.2$, and (c) $\delta = 0.4$.

In Cases F–H where the objective function is J_{h_p}, we hardly observe the effect of the embedding dimension D_e on $\overline{K}$. In the following, we set $D_e = 4$ for all the cases.

Figure 4 shows the maps of $\overline{K}$ and $\overline{h_p}$ as functions of σ and δ in the uncontrolled case and optimal control cases for J_K and J_{h_p}. In the uncontrolled case as shown in Figs. 4(a) and 4(b), $\overline{K}$ increases monotonically with δ, especially in the

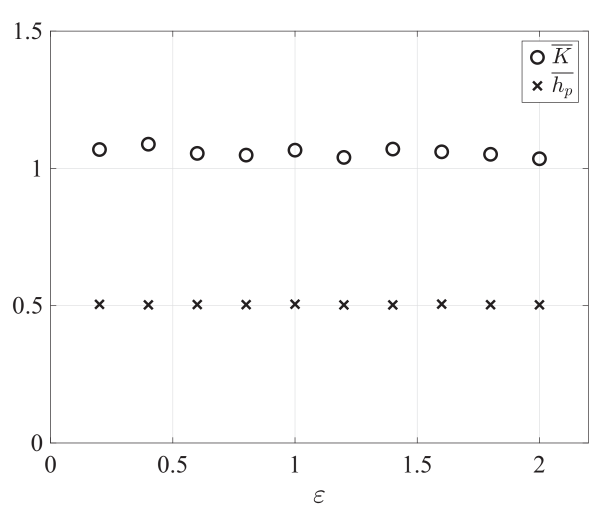

FIG. 3. Impulse-response test for the J_{h_p} case at $D_e = 4$, N_{iter}=4, $T_{\mathrm{opt}} = 0.4$, and $T_a = 0.2$.

TABLE II. Parameter sets for investigating the effect of optimization parameters at $\delta = 0.2$, $\sigma = 1.0$, and $\nu = 1$.

	Objective function	D_e	N_{iter}	T_{opt}	T_a	$\overline{K}$	$\overline{h_p}$
	No control	3				1.08	0.617
	No control	4				1.09	0.501
	No control	5				1.08	0.440
Case A	J_K	4	2	0.4	0.2	0.178	0.446
Case B	J_K	4	3	0.4	0.2	0.175	0.454
Case C	J_K	4	4	0.4	0.2	0.174	0.460
Case D	J_K	4	3	0.8	0.4	1.49×10^{-3}	0.611
Case E	J_K	4	3	0.4	0.1	0.158	0.461
Case F	J_{h_p}	3	3	0.4	0.2	1.05	0.617
Case G	J_{h_p}	4	3	0.4	0.2	1.06	0.501
Case H	J_{h_p}	5	3	0.4	0.2	1.06	0.447

TABLE III. Variations in $\overline{K}$, $\overline{F}$, and $\overline{h_p}$ in six different cases.

	Cost Function	δ	ν	σ	$\overline{K}$	$\overline{F}$	$\overline{h_p}$
Case 1		0.2	1.0	1.0	1.09		0.501
Case 2	J_K	0.2	1.0	1.0	0.18	3.36×10^{-2}	0.455
Case 3	J_{h_p}	0.2	1.0	1.0	1.06	1.14×10^{-6}	0.505
Case 4		0.6	1.0	5.0	1.68		0.516
Case 5	J_K	0.6	1.0	5.0	0.23	4.32×10^{-2}	0.525
Case 6	J_{h_p}	0.6	1.0	5.0	1.58	9.30×10^{-7}	0.510

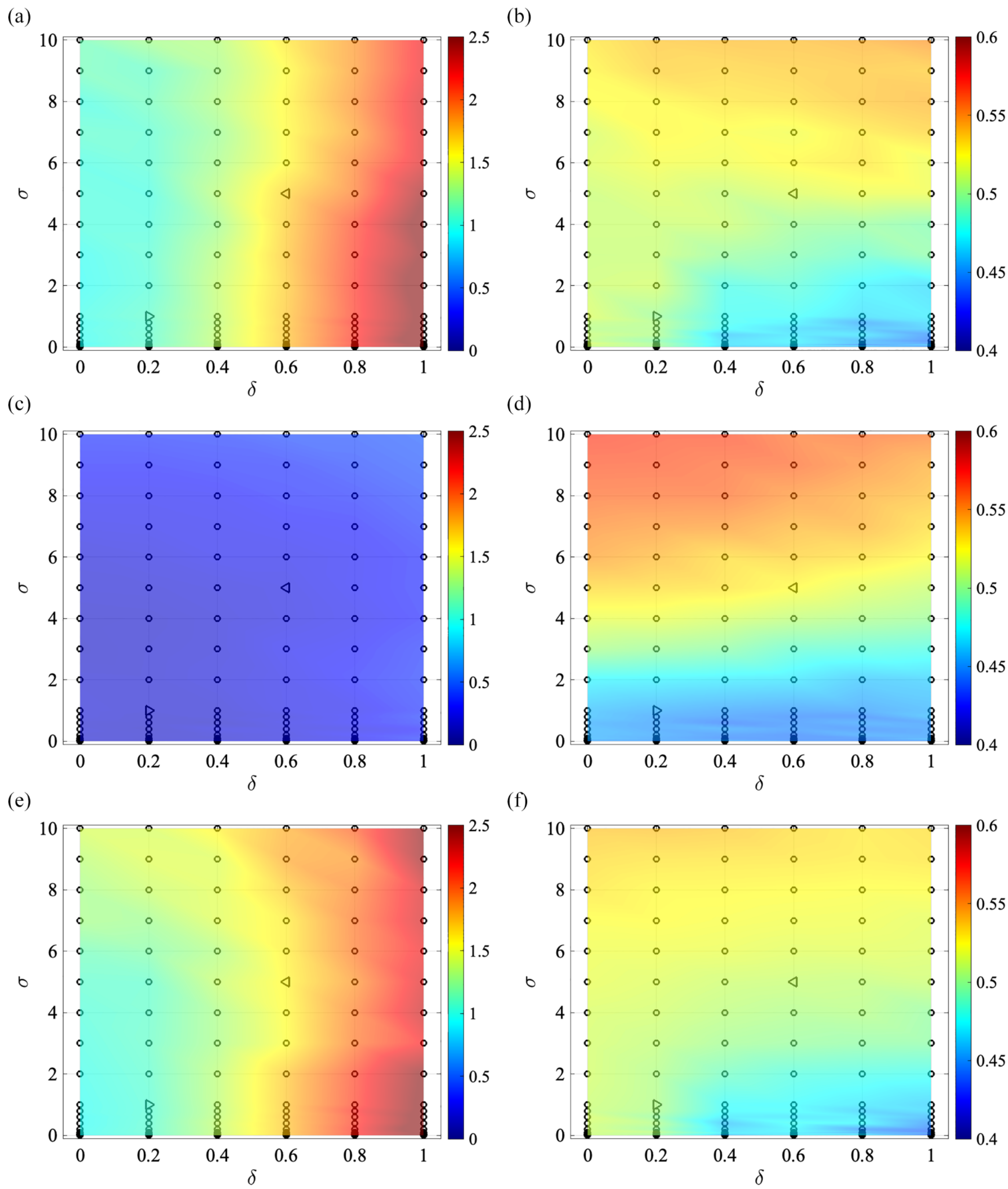

FIG. 4. Maps of $\overline{K}$ (left) and $\overline{h_p}$ (right) as functions of σ and δ: top, uncontrolled case; middle, optimal control for J_K; bottom, optimal control for J_{h_p}. Each circle represents a single simulation and triangles indicate reference cases in Table III.

high-δ and low-σ region. However, h_p slightly decreases in the high-δ, low-σ corner. For the case of J_K in Figs. 4(c) and 4(d), $\overline{K}$ is significantly suppressed across the entire parameter space and $\overline{h_p}$ is reduced for small σ. Conversely, in the case of J_{h_p} in Figs. 4(e) and 4(f), $\overline{K}$ and $\overline{h_p}$ are slightly reduced compared to the uncontrolled case.

Table III presents a comparative evaluation of the control effects under different cost functionals. The control cost F is defined as

$$\overline{F} = \frac{1}{L_x(\mathcal{T}_2 - \mathcal{T}_1)} \int_{\mathcal{T}_1}^{\mathcal{T}_2} \int_0^{L_x} \frac{f^2}{2}\, dx\, dt. \tag{14}$$

Cases 1–3 are the small δ and σ cases. In Case 2 where the cost function is J_K, $\overline{K}$ is significantly reduced from 1.09 to 0.18 with a moderate control cost $\overline{F}$, accompanying the reduction of $\overline{h_p}$. In contrast, in Case 3 where the cost function is J_{h_p}, the reduction of $\overline{K}$ is small and $\overline{h_p}$ maintains the level of Case 1. A similar trend is observed in the large δ and σ in Cases 4–6. In Case 5, the control based on J_K achieves a substantial reduction in $\overline{K}$, while maintaining a comparable h_p level, though it requires a higher control cost F. In Case 6, optimization for J_{h_p} yields a small decrease in $\overline{K}$, while maintaining h_p and almost negligible control cost. While the control cost $\overline{F}$

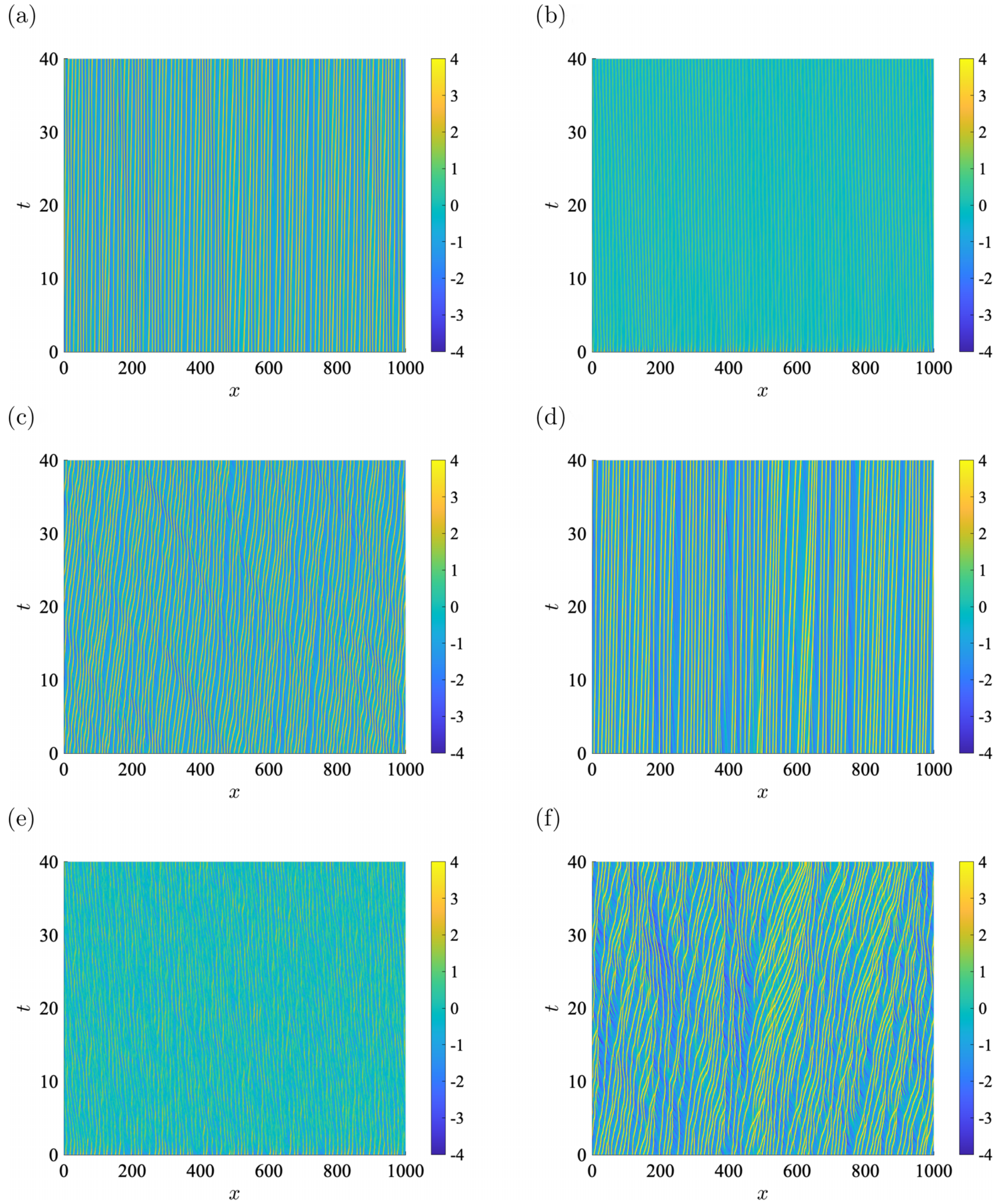

FIG. 5. Spatiotemporal patterns in (a) Case 1, (b) Case 2, (c) Case 3, (d) Case 4, (e) Case 5, and (f) Case 6.

is very small in Cases 3 and 6, the spatiotemporal patterns are not identical to those of the corresponding uncontrolled cases (as discussed later). Although the dominant structures are preserved, their regularity is modified, indicating that the J_{h_p}-based control induces a weak but nontrivial reorganization of the dynamics.

Figure 5 visualizes the spatiotemporal patterns of the system state for Cases 1–6. In the uncontrolled cases (Case 1 and Case 4), we observe coherent structures, suggesting the dominance of low-frequency modes and sustained spatial correlations. Notably, the inclination becomes steeper in Case 4 due to the larger values of δ and σ, indicating more energetic dynamics. Under optimal control for J_K, both Case 2 and Case 5 markedly exhibit the suppression of spatiotemporal structures. In Case 2, the pattern becomes nearly uniform, consistent with the significant reduction in kinetic energy shown in Table III. This indicates that the control successfully suppresses the spatiotemporal structures. These results suggest that energy minimization through the optimized external forcing has a dampinglike effect on the system. It should be emphasized, however, that the optimized forcing is not equivalent to modifying the damping coefficient of the governing equation. In Case 5, spatial coherence is similarly disrupted and the small fluctuations remain, reflecting the larger $\overline{K}$ and

$\overline{F}$ than Case 2. In Cases 3 and 6 with the optimal control for J_{h_p}, in contrast, the spatial structure remains. However, the structures are less regular, especially in Case 6, where a more complex distribution is observed.

Overall, the optimal control for J_K significantly reduces the kinetic energy while it requires a large energy input. The coherent structures are significantly suppressed. On the other hand, the optimal control for J_{h_p} slightly reduces the kinetic energy. However, the system retains an h_p level similar to that of the uncontrolled case without destroying the coherent structure, while requiring little cost function.

The present results show that minimizing energy and minimizing entropy lead to qualitatively different controlled states. This suggests that energy and entropy characterize different aspects of the system dynamics and are not necessarily in one-to-one correspondence.

IV. SUMMARY

This study demonstrates the effectiveness of optimal control for spatiotemporal dynamics governed by the noisy generalized Kuramoto-Sivashinsky equation through numerical simulations. In the control based on J_K, the kinetic energy is significantly reduced and the permutation entropy decreases. In the control based on h_p, the reduction of kinetic energy is small and the entropy maintains the level of the uncontrolled case, while the control cost is significantly small.

These findings highlight an important trade-off between energy minimization and informational richness in the system dynamics. While the control based on J_K is effective in reducing the kinetic energy, it leads to a near-complete suppression of spatiotemporal structures, resulting in a highly ordered trivial state in the extreme case. Such "dead" states may be acceptable or even desirable in certain applications, where structural activity is inherently wasteful. However, in other contexts where spatiotemporal structure plays a functional role, a completely ordered state can be detrimental. In contrast, the control based on J_{h_p}, which preserves a higher level of entropy, allows the system to maintain structural diversity while still achieving modest energy savings with minimal control cost. This indicates that the system retains its dynamical richness and is not driven into an overly suppressed regime. Therefore, when the objective is not only to reduce energy but also to maintain meaningful structure in the system, entropy-preserving control is a promising strategy.

Extending this framework to three-dimensional turbulent flows governed by the Navier-Stokes equations is an important direction for future work, although it would substantially increase the computational cost of both the forward and adjoint simulations. Such an extension is feasible in principle, while its computational scalability remains to be systematically examined. As a next step, the present approach could be applied to turbulent flows over a finite optimization horizon to compare energy- and entropy-based objectives. This would clarify whether entropy minimization can produce controlled turbulent states that are qualitatively different from those obtained by conventional energy-based optimization.

ACKNOWLEDGMENT

This study was partially supported by the Ministry of Education, Culture, Sports, Science, and Technology through a Grant-in-Aid for Scientific Research (S) (No. 21H05007), and Early-Career Scientists (No. 25K17542).

DATA AVAILABILITY

The processed numerical data, analysis scripts, and individual figure files that support the findings of this article are publicly available [12].

[1] Y. Kuramoto and T. Tsuzuki, Persistent propagation of concentration waves in dissipative media far from thermal equilibrium, Prog. Theor. Phys. **55**, 356 (1976).
[2] G. Sivashinsky, Nonlinear analysis of hydrodynamic instability in laminar flames–I. Derivation of basic equations, Acta Astronaut. **4**, 1177 (1977).
[3] H. Gotoda, M. Pradas, and S. Kalliadasis, Nonlinear forecasting of the generalized kuramoto-sivashinsky equation, Int. J. Bifurc. Chaos **25**, 1530015 (2015).
[4] H. Gotoda, M. Pradas, and S. Kalliadasis, Chaotic versus stochastic behavior in active-dissipative nonlinear systems, Phys. Rev. Fluids **2**, 124401 (2017).
[5] T. R. Bewley, P. Moin, and R. Temam, DNS-based predictive control of turbulence: An optimal benchmark for feedback algorithms, J. Fluid Mech. **447**, 179 (2001).
[6] A. Yamamoto, Y. Hasegawa, and N. Kasagi, Optimal control of dissimilar heat and momentum transfer in a fully developed turbulent channel flow, J. Fluid Mech. **733**, 189 (2013).
[7] J. M. Amigó, *Permutation Complexity in Dynamical Systems* (Springer, Berlin, 2010).
[8] C. Bandt and B. Pompe, Permutation entropy: A natural complexity measure for time series, Phys. Rev. Lett. **88**, 174102 (2002).
[9] K. Fukagata, N. Kasagi, and P. Koumoutsakos, A theoretical prediction of friction drag reduction in turbulent flow by superhydrophobic surfaces, Phys. Fluids **18**, 051703 (2006).
[10] F. Ham, F. Lien, and A. Strong, A fully conservative second-order finite difference scheme for incompressible flow on nonuniform grids, J. Comput. Phys. **177**, 117 (2002).
[11] K. Fukagata and N. Kasagi, Highly energy-conservative finite difference method for the cylindrical coordinate system, J. Comput. Phys. **181**, 478 (2002).
[12] H. Mamori, Y. Nabae, and H. Gotoda, Optimal control of the generalized Kuramoto–Sivashinsky equation with energy- and entropy-based objectives [Dataset], The University of Electro-Communications open-data-hub, 2026, https://open-data-hub.office.uec.ac.jp/s/7EtCGwytGBNGTN4.